Energy Conversion and Management 52 (2011) 876–883

Contents lists available at ScienceDirect

Energy Conversion and Management

journal homepage: www.elsevier.com/locate/enconman

# Numerical analysis on the performance of solar chimney power plant system

Guoliang Xu, Tingzhen Ming *, Yuan Pan, Fanlong Meng, Cheng Zhou

*School of Energy and Power Engineering, Huazhong University of Science and Technology, Wuhan 430074, China*

ARTICLE INFO

*Article history:*
Received 2 January 2010
Accepted 15 August 2010
Available online 9 September 2010

*Keywords:*
Solar chimney power plant system
Collector
Energy storage layer
Chimney
Turbine

ABSTRACT

Power generating technology based on renewable energy resources will definitely become a new trend of future energy utilization. Numerical simulations on air flow, heat transfer and power output characteristics of a solar chimney power plant model with energy storage layer and turbine similar to the Spanish prototype were carried out in this paper, and mathematical model of flow and heat transfer for the solar chimney power plant system was established. The influences of solar radiation and pressure drop across the turbine on the flow and heat transfer, output power and energy loss of the solar chimney power plant system were analyzed. The numerical simulation results reveal that: when the solar radiation and the turbine efficiency are 600 W/m$^2$ and 80%, respectively, the output power of the system can reach 120 kW. In addition, large mass flow rate of air flowing through the chimney outlet become the main cause of energy loss in the system, and the collector canopy also results in large energy loss.



## 1. Introduction

Because of the pressure of reducing carbon dioxide emissions, it becomes more and more urgent for China to carry out various applications and researches on new energy generating technologies. The solar chimney power plant system (SC), which has the following advantages while compared with the traditional power generating systems: easier to design, more convenient to draw materials, higher operational reliability, fewer running components, more convenient maintenance and overhaul, and lower maintenance expense, no environmental contamination, continuous stable running, longer operational life span, was first proposed in the late 1970s by professor Jörg Schlaich and tested with a prototype model in Manzanares, Spain in the early 1980s [1,2]. It has the potential to meet the power needs of developing countries and territories, especially in deserts where electric power is in shortage, and has extensive prospect of application.

As the SC systems could make significant contributions to the energy supplies of those countries where there is plenty of desert land, which is not being utilized, in recent years, many researchers have made research reports on this technology and have carried out tracking study on SC systems. Haaf et al. [1,2] provided fundamental studies for the Spanish prototype in which the energy balance, design criteria and cost analysis were discussed and report on preliminary test results of the SC system was made. Some small scale solar chimney devices with power outputs no more than 10 W were also reported but could only validate the feasibility and principle of the solar chimney system [3,4].

Different mathematical models based on 1-D thermal equilibrium were advanced by several researchers [5–8], Pasumarthi and Sherif [5] developed a mathematical model to study the effects of various environment conditions and geometry on the flow and heat transfer characteristics and output power of the solar chimney. Bernardes et al. [6] established a rounded mathematic model including the collector, chimney, turbine of SC system on the basis of energy-balance principle. Bilgen and Rheault [7] designed a SC system for power production at high latitudes and evaluated its performance. Pretorius and Kröger [8] evaluated the influence of a developed convective heat transfer equation, more accurate turbine inlet loss coefficient, quality collector roof glass and various types of soil on the performance of a large scale SC system.

Gannon and Von Backström [9] presented an air standard cycle analysis of the SC for the calculation of limiting performance, efficiency, and relationship between main variables including chimney friction, system, turbine and exit kinetic energy losses. Gannon and Von Backström [10] presented an experimental investigation of the performance of a solar chimney turbine. The measured results showed that the solar chimney turbine presented has a total-to-total efficiency of 85–90% and total-to-static of 77–80% over the design range. Later, the same authors [11] presented analytical equations in terms of turbine flow and load coefficient and degree of reaction, to express the influence of each coefficient on turbine efficiency.

Pastohr et al. [12] carried out two-dimensional steady-state numerical simulation study on the whole SC system which consists of energy storage layer, collector, turbine and the chimney, and obtained the distributions of velocity, pressure and temperature inside the collector. Ming et al. [13] developed a comprehensive model to evaluate the performance of a SC system, in which the

* Corresponding author.
*E-mail address:* mtzhen@163.com (T. Ming).

0196-8904/$ - see front matter © 2010 Elsevier Ltd. All rights reserved.
doi:10.1016/j.enconman.2010.08.014

**Nomenclature**

| | |
|---|---|
| $u$ | average velocity magnitude in the axial direction (m/s) |
| $r$ | co-ordinate in radial direction (m) |
| $T$ | temperature (K) |
| $T_0$ | temperature of the environment (K) |
| $g$ | gravity, $g$ = 9.807 (m/s$^2$) |
| Pr | Prandtl number (dimensionless), $\mathrm{Pr} = \frac{c_p \mu}{k}$ |
| $x$ | co-ordinate in axial direction (m) |
| $S_\phi$ | source item |

*Greek symbols*

| | |
|---|---|
| $v$ | kinematic viscosity (m$^2$/s) |
| $\mu_t$ | turbulent dynamic viscosity coefficient |
| $\mu$ | dynamic viscosity (kg/m s) |
| $\beta$ | coefficient of cubic expansion |
| $\rho$ | density (kg/m$^3$) |
| $\kappa$ | turbulent kinetic energy (J/kg) |
| $\varepsilon$ | dissipation (W/kg) |
| $\sigma_\varepsilon$ | Prandtl number of dissipation |
| $\sigma_T$ | Prandtl number of turbulence |
| $\sigma_\kappa$ | Prandtl number of pulse kinetic energy 1.0 |
| $\Gamma_\phi$ | generalized diffusion coefficient |

*Subscripts*

| | |
|---|---|
| $e$ | environment |
| $t$ | viscous dissipation effect caused by turbulent characteristics |
| $\varepsilon$ | dissipation |
| $\kappa$ | kinetic energy |
| $\phi$ | porosity |
| $T$ | turbulent flow |

effects of various parameters on the relative static pressure, driving force, power output and efficiency have been further investigated. Ming et al. [14] established different mathematical models for the collector, the chimney and the energy storage layer and analyzed the effect of solar radiation on the heat storage characteristic of the energy storage layer. Ming et al. [15] carried out numerical simulations on the SC systems coupled with a 3-blade turbine using the Spanish prototype as a practical example and presented design and simulation of a MW-graded SC system with a 5-blade turbine, the results of which show that the coupling of turbine increases the maximum power output of the system and the turbine efficiency is also relatively rather high.

The previous research reports indicate that, provided the considerable scale of SC system, carrying out numerical simulation for it before setting up the commercial system would be an effective method to make prediction of the characteristic parameters and operating characteristics of the system. Apparently, mathematical models based on 1-D thermal equilibrium can not give detailed descriptions on the temperature, velocity and pressure distributions of the whole systems. During the two-dimension simulation for SC system carried out by Pastohr et al. [12], the pressure drop across the turbine was preset according to the Beetz power limit theory, as the turbine of the SC system is pressure-based which is similar to the turbine of a hydraulic power station but different from that of a traditional wind power station, therefore, different pressure drops across the turbine can be preset to analyze the power output characteristic of the SC system. In addition, the existing numerical simulation results of Ref. [12–15] did not analyze the influences of solar radiation, turbine pressure drop and efficiency on the flow and heat transfer, output power and energy loss of the SC system. Based on this, two-dimension numerical simulations for the Spanish solar chimney power plant prototype containing all the key parts such as energy storage layer, collector, turbine and the chimney will be carried out in this paper to analyze the influences of the solar radiation, turbine pressure drop and turbine efficiency on following items such as flow, heat transfer, energy loss and power output characteristics of the SC system.

## 2. Theoretical models

### 2.1. Physics model

A SC system with the same fundamental dimensions as the Spanish SC prototype will be built in Wuhan, China. Taking the fundamental dimensions of the Spanish SC system shown in Fig. 1 as a practical example [2], geometric parameters of the prototype are shown as follows: height of chimney, 200 m; diameter of chimney, 10 m; radius of collector, 122 m; height from the inlet to its center, 2–6 m; thickness of the energy storage layer, 5 m. The collector and the chimney are smoothly connected in order to reduce the energy loss caused by resistance, besides, shrink flow passage is designed at the bottom of collector. The material applied for the collector canopy is transparent glass, while the energy storage layer applies the soil that can be regarded as porous media.

### 2.2. Mathematical model

In natural convection, the strength of the buoyancy-induced flow is measured by the Rayleigh number defined as follows:

$$\mathrm{Ra} = \frac{g\beta\Delta T L^3}{av} \tag{1}$$

where $\Delta T$ is the maximum temperature difference of the system. $L$, $a$ and $\beta$ are the mean collector height and the thermal diffusivity

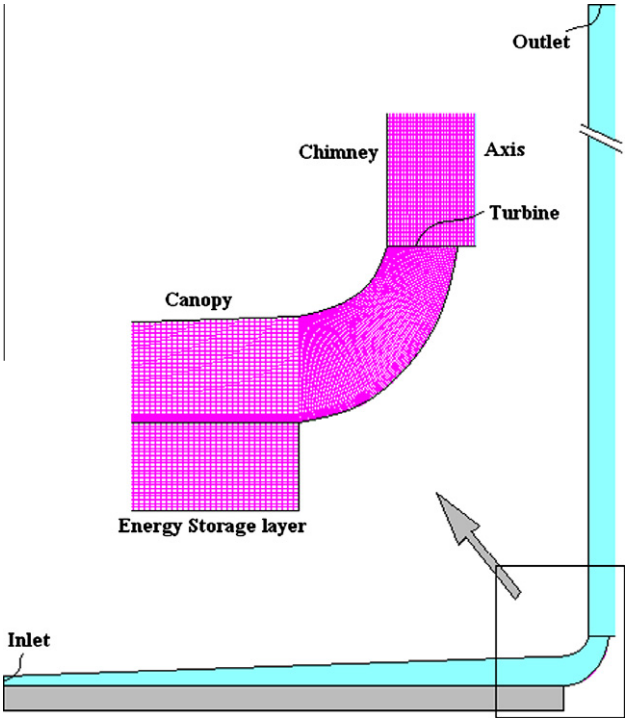


**Fig. 1.** Physical model of the SC prototype.

and the thermal expansion coefficient, respectively. In the whole collector and chimney analysis shows that $Ra > 10^{10}$, thereby, fluid flow in the regions may be turbulence. Accordingly, the axisymmetric mathematical model including the continuity equation, Navier–Stocks equation, energy equation and $\kappa$–$\varepsilon$ equations to describe the problem are as follows:

$$\frac{\partial(\rho u)}{\partial x}+\frac{1}{r}\frac{\partial(r\rho v)}{\partial r}=0 \tag{2}$$

$$\begin{aligned}\frac{\partial}{\partial x}(\rho uu)+\frac{1}{r}\frac{\partial}{\partial r}(r\rho vu)=&\frac{\partial}{\partial x}\left((\mu+\mu_t)\frac{\partial u}{\partial x}\right)+\frac{1}{r}\\&\times\frac{\partial}{\partial r}\left((\mu+\mu_t)r\frac{\partial u}{\partial r}\right)+\rho g\beta(T-T_0)\\&+\frac{\partial}{\partial x}\left((\mu+\mu_t)\frac{\partial u}{\partial x}\right)+\frac{1}{r}\\&\times\frac{\partial}{\partial r}\left((\mu+\mu_t)r\frac{\partial v}{\partial x}\right)\end{aligned} \tag{3}$$

$$\begin{aligned}\frac{\partial}{\partial x}(\rho uv)+\frac{1}{r}\frac{\partial}{\partial r}(r\rho vv)=&\frac{\partial}{\partial x}\left((\mu+\mu_t)\frac{\partial v}{\partial x}\right)+\frac{1}{r}\\&\times\frac{\partial}{\partial r}\left((\mu+\mu_t)r\frac{\partial v}{\partial r}\right)+-\frac{\partial p}{\partial r}\\&+\frac{\partial}{\partial x}\left((\mu+\mu_t)\frac{\partial u}{\partial r}\right)+\frac{1}{r}\\&\times\frac{\partial}{\partial r}\left((\mu+\mu_t)r\frac{\partial v}{\partial x}\right)-\frac{2(\mu+\mu_t)v}{r^2}\end{aligned} \tag{4}$$

$$\begin{aligned}\frac{\partial(uT)}{\partial x}+\frac{1}{r}\frac{\partial(rvT)}{\partial r}=&\frac{1}{\rho}\frac{\partial}{\partial x}\left(\left(\frac{\mu}{\mathrm{Pr}}+\frac{\mu_t}{\sigma_T}\right)\frac{\partial T}{\partial x}\right)+\frac{1}{\rho r}\\&\times\frac{\partial}{\partial r}\left(\left(\frac{\mu}{\mathrm{Pr}}+\frac{\mu_t}{\sigma_T}\right)r\frac{\partial T}{\partial r}\right)\end{aligned} \tag{5}$$

$$\begin{aligned}\frac{\partial(u\kappa)}{\partial x}+\frac{1}{r}\frac{\partial(rv\kappa)}{\partial r}=&\frac{1}{\rho}\frac{\partial}{\partial x}\left(\left(\mu+\frac{\mu_t}{\sigma_\kappa}\right)\frac{\partial \kappa}{\partial x}\right)+\frac{1}{\rho r}\\&\times\frac{\partial}{\partial r}\left(\left(\mu+\frac{\mu_t}{\sigma_\kappa}\right)r\frac{\partial \kappa}{\partial r}\right)+G_\kappa-\varepsilon\end{aligned} \tag{6}$$

$$\begin{aligned}\frac{\partial(u\varepsilon)}{\partial x}+\frac{1}{r}\frac{\partial(rv\varepsilon)}{\partial r}=&\frac{1}{\rho}\frac{\partial}{\partial x}\left(\left(\mu+\frac{\mu_t}{\sigma_\varepsilon}\right)\frac{\partial \varepsilon}{\partial x}\right)+\frac{1}{\rho r}\\&\times\frac{\partial}{\partial r}\left(\left(\mu+\frac{\mu_t}{\sigma_\varepsilon}\right)r\frac{\partial \varepsilon}{\partial r}\right)+\frac{\varepsilon}{\kappa}(C_1G_\kappa-C_2\varepsilon)\end{aligned} \tag{7}$$

where $G_\kappa$ represents the generation of turbulence kinetic energy due to the mean velocity gradients defined as: $G_\kappa=-\mu_t\left(2\left(\left(\frac{\partial u}{\partial x}\right)^2+\left(\frac{\partial v}{\partial r}\right)^2+\left(\frac{v}{r}\right)^2\right)+\left(\frac{\partial u}{\partial r}+\frac{\partial v}{\partial x}\right)^2\right)$. $\sigma_T$, $\sigma_\kappa$ and $\sigma_\varepsilon$ are the turbulent Prandtl numbers for $T$, $\kappa$ and $\varepsilon$ respectively, and $c_1$ and $c_2$ are two constant for turbulent model: $c_1 = 1.44$, $c_2 = 1.92$, $\sigma_T = 0.9$, $\sigma_\kappa = 1.0$, $\sigma_\varepsilon = 1.3$. $\mu_t=\frac{c_\mu\rho\kappa^2}{\varepsilon}$, and $c_\mu = 0.09$.

The heat transfer and flow in the energy storage layer may be very complicated, and it is necessary to take into account of the collector, the chimney and the storage medium as a whole system. As the material used for energy storage layer can be regarded as porous medium, the Brinkman–Forchheimer Extended Darcy model [16] is used to describe the flow in the convective porous-layer, which can be expressed as follows:

$$\frac{\partial u}{\partial x}+\frac{1}{r}\frac{\partial(rv)}{\partial r}=0 \tag{8}$$

$$\begin{aligned}&\frac{\rho}{\varphi}\frac{\partial u}{\partial t}+\frac{\rho}{\varphi^2}\left(\frac{\partial(uu)}{\partial x}+\frac{1}{r}\frac{\partial(rvu)}{\partial r}\right)\\&=-\frac{\partial p}{\partial x}+\frac{\partial}{\partial x}\left(\mu_m\frac{\partial u}{\partial x}\right)+\frac{1}{r}\frac{\partial}{\partial r}\left(r\mu_m\frac{\partial u}{\partial r}\right)-\frac{\mu u}{K}-\frac{\rho F}{\sqrt{K}}\\&\quad\times\sqrt{u^2+v^2}u+\rho g\beta(T-T_e)\end{aligned} \tag{9}$$

$$\begin{aligned}&\frac{\rho}{\varphi}\frac{\partial v}{\partial t}+\frac{\rho}{\varphi^2}\left(\frac{\partial(uv)}{\partial z}+\frac{1}{r}\frac{\partial(rvv)}{\partial r}\right)\\&=\frac{\partial}{\partial z}\left(\mu_m\frac{\partial v}{\partial z}\right)+\frac{1}{r}\frac{\partial}{\partial r}\left(r\mu_m\frac{\partial v}{\partial r}\right)-\mu_m\frac{v}{r^2}-\frac{\mu u}{K}-\frac{\rho F}{\sqrt{K}}\\&\quad\times\sqrt{u^2+v^2}v\end{aligned} \tag{10}$$

$$\rho_m c_{p,m}\left(\frac{\partial T}{\partial t}+\frac{\partial(uT)}{\partial z}+\frac{1}{r}\frac{\partial(rvT)}{\partial r}\right)=\frac{\partial}{\partial z}\left(\lambda_m\frac{\partial T}{\partial z}\right)+\frac{1}{r}\frac{\partial}{\partial r}\left(r\lambda_m\frac{\partial T}{\partial r}\right) \tag{11}$$

where $\phi$, $\rho_m$, $c_{p,m}$, $\mu_m$ and $\lambda_m$ are the porosity, apparent density, specific capacity, dynamic viscosity and apparent thermal conductivity of the porous medium, respectively: $\rho_m = (1-\phi)\rho_s + \phi\rho_a$, $c_{p,m} = (1-\phi)c_{p,s} + \phi c_{p,a}$, $\lambda_m = (1-\varphi)\lambda_s + \varphi\lambda_a$, $\mu_m = \mu/\phi$, the parameters with subscripts $s$ and $a$ denote the corresponding parameters of the solid and air in the energy storage layer, respectively. $K$, $F$ and $d_b$ are the permeability, the inertia coefficient and the particle diameter of the energy storage layer, respectively.

$$K=d_b^2\varphi^3/(175(1-\varphi)^2) \tag{12}$$

$$F=1.75\varphi^{-1.5}/\sqrt{175} \tag{13}$$

### 2.3. Boundary conditions and solution method

Boundary conditions are set as follows: for the roof of collector, we take convection boundary into account, and coefficient of convection is set as 10 W/(m$^2$ K) which can be accepted when the environment air velocity is not very large, i.e. 1–2 m/s. The temperature of the environment is set as 293 K, inlet of collector is set as the pressure-inlet boundary, the chimney wall can be set as an adiabatic boundary; the chimney outlet is set as pressure-outlet boundary; the bottom of the energy storage layer is set as temperature-constant boundary, whose temperature is 300 K. Solar radiation which projects through the transparent ceiling into the ground can be considered as a heat source for the ground thin layer [12]. In recent years, the highest solar radiation in Wuhan area is about 650 W, therefore, we can simulate the running conditions of a SC system in Wuhan on the whole by setting solar radiation as 200 W/m$^2$, 400 W/m$^2$, 600 W/m$^2$ and 800 W/m$^2$, respectively.

In addition, it is necessary to explain the reason for which we consider the collector inlet and chimney outlet both as pressure boundaries and have their pressures set as 0 Pa is that we simultaneously take the inner and outer pressure distributions of the system into account [12,13], $p_{r,i} = 0$ means that for both the inside and outside of the collector inlet, the static pressures at the same height are the same.

However, the setting of pressure drop across the turbine in this paper differs from the processing method applied by Pastohr [12]. The turbine of SC system, as explained earlier above, belongs to a pressure-based wind turbine, the fore-and-aft air velocities are almost the same but the pressure changes significantly, and its power output does not follow the Beetz power limit theory. Thereby the output power through the turbine can be calculated according to Eq. (14) by presetting the pressure drop across the turbine:

$$W_t=\eta_t\cdot\Delta p\cdot V \tag{14}$$

where $W_t$ represents the shaft power output through the turbine, $\eta_t$ represents the energy conversion efficiency of the turbine, which can be preset as 80%, less than the optimized data [10,11], $\Delta p$ represents the pressure drop across the turbine, $V$ represents the air volume flow rate of the system flowing through the chimney outlet. The boundary conditions for different places are shown in Table 1.

Standard $k$–$\varepsilon$ model is applied during the numerical simulation of air flow in the collector and chimney, The material for the energy

**Table 1**
Boundary conditions.

| Place | Type | Value |
|---|---|---|
| 0.1 mm top layer of the ground | Heat source | 2–8 × $10^6$ W/m$^3$ |
| Bottom of the ground | Temperature | 300 K |
| Surface of the canopy | Wall | $T_e$ = 293 K, $h$ = 10 W/(m$^2$ K) |
| Surface of the chimney | Wall | $q_{chim}$ = 0 W/m$^2$ |
| Collector inlet | Pressure inlet | $p_{r,i}$ = 0 Pa, $T_0$ = 293 K |
| Chimney outlet | Pressure outlet | $p_{r,o}$ = 0 Pa |
| Pressure drop across the turbine | Reverse fan | 0–480 Pa, 40 Pa in interval |

storage layer is selected as soil, and the properties of the soil are as follows: $\rho_{soil}$ = 1700 kg/m$^3$, $c_{p,soil}$ = 2016 J/(kg K), $\lambda_{soil}$ = 0.78 W/(m K). The porosity of the energy storage layer are selected as 0.1 as in Wuhan, China, the soil is almost close-grained. Standard wall function method is applied, SIMPLE algorithm is applied for the couple of pressure–velocity, and the momentum equation, energy equation and other equations all apply the 2nd-order upwind discretization scheme. The mesh number of the SC system is nearly 500,000, where we can get a grid-independent simulation result. The general commercial soft Fluent 6.2 is used to carry out the numerical simulation process [17].

## 3. Validity

Comparison between the numerical simulation results and the experimental results collected on 2nd September, 1982 of the Spanish SC system is carried out in order to verify the validity of the numerical simulation results in this paper. The computation parameters are set according to literature [2], and solar radiation and ambient parameters are set as key conditions for the numerical simulation. As indicated in Fig. 2, the simulation results are quite consistent with the experimental results, in detail, simulation results fluctuate slightly but its curve is relatively quite smooth, besides, its difference from the experimental results is less than 5%, simulation results is slightly higher than experimental results at noon, which is because the ambient wind velocity was not measured, while when we consider the collector canopy's heat dissipation we assume that the ambient wind velocity is just 2 m/s, which may have underestimated the heat dissipation from the system to the ambience. Hence it can be concluded that the numerical simulation method applied in this paper is effective and feasible.

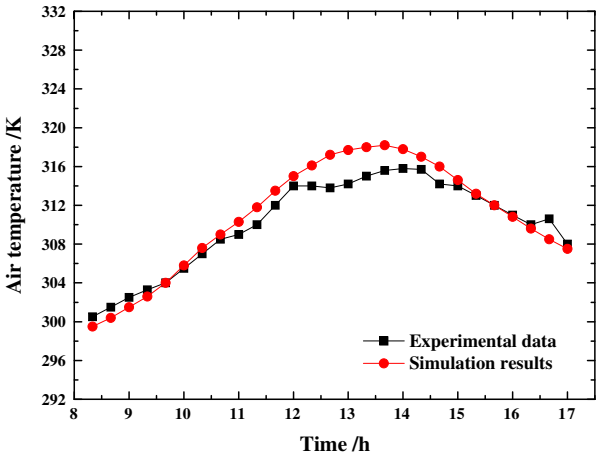


**Fig. 2.** Comparison between numerical simulation results and experimental results.

## 4. Results and discussion

Currently, solar power plant and wind power plant are the main power generating systems using renewable energy, namely solar power and wind power respectively. Turbines applied in SC system and wind power plant are pressure-based impulse turbine and velocity-based impulse turbine respectively. For the former system where the air flow is subjected to the area of the chimney, fore-and-aft velocity changes little accompanied with pressure drop, as for the latter one, fore-and-aft pressure changes little while the velocity decreases significantly.

Figs. 3–5 show the simulation results on flow and heat transfer characteristics of the SC system when solar radiation and pressure drop across the turbine are 400 W/m$^2$ and 0 Pa (when turbine is not in service) respectively. As shown in Fig. 3, relative static pressure (defined as the difference between the inner-system static

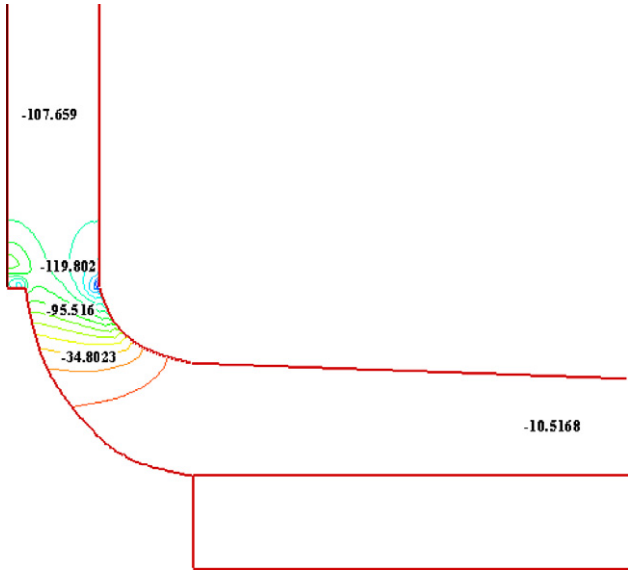


**Fig. 3.** Relative static pressure distribution when the solar radiation and pressure drop across the turbine are 400 W/m$^2$ and 0 Pa, respectively (Pa).

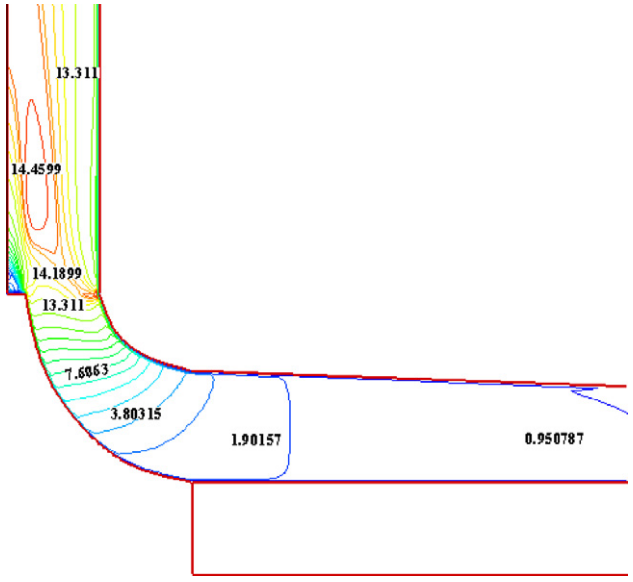


**Fig. 4.** Velocity distribution when the solar radiation and pressure drop across the turbine are 400 W/m$^2$ and 0 Pa, respectively (m/s).

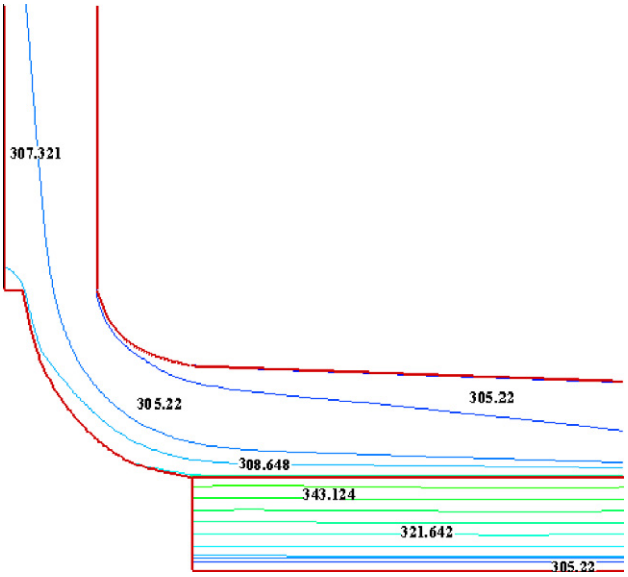


**Fig. 5.** Temperature distribution when the solar radiation and pressure drop across the turbine are 400 W/m$^2$ and 0 Pa, respectively (K).

pressure and the environment static pressure at the same height) inside the system has negative values everywhere, this indicates that pressure inside the system is always lower than that of the environment. Among this, the pressure difference between the chimney bottom and the environment comes to the maximum. Meanwhile, the velocity also reaches its maximum which is over 12 m/s. On the other hand, temperature inside the system increases up to 307 K, which experiences a 15 K change compared with the environment temperature. Obviously, under no-load condition, this temperature variation is not very dramatic.

Fig. 6–9 show the simulation results on flow and heat transfer characteristics of the SC system when solar radiation and pressure drop across the turbine are 400 W/m$^2$ and 120 Pa respectively. It is found that, compared with Figs. 6 and 7 and Fig. 3, the pressure distribution inside the system has experienced dramatic variations, among which the pressure drop within the turbine area is extremely dramatic, this is because the turbine is preset a 120 Pa pressure drop during this numerical simulation, and the results as shown in Figs. 6 and 7 exactly reflect this effect.

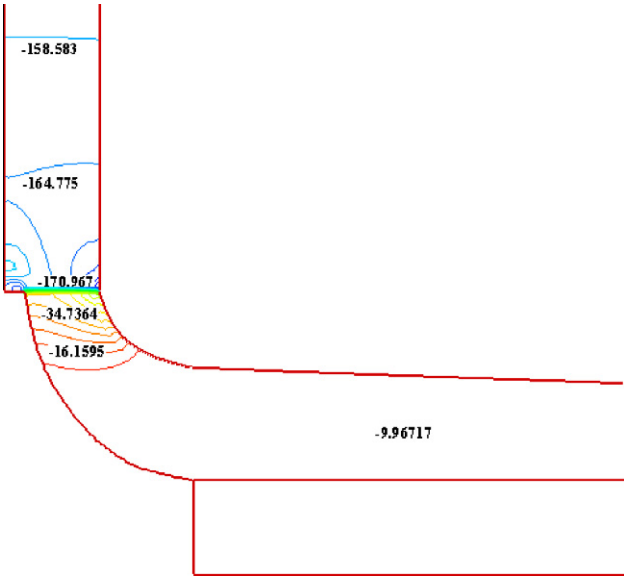


**Fig. 6.** Relative static pressure distribution when the solar radiation and pressure drop across the turbine are 400 W/m$^2$ and 120 Pa, respectively (Pa).

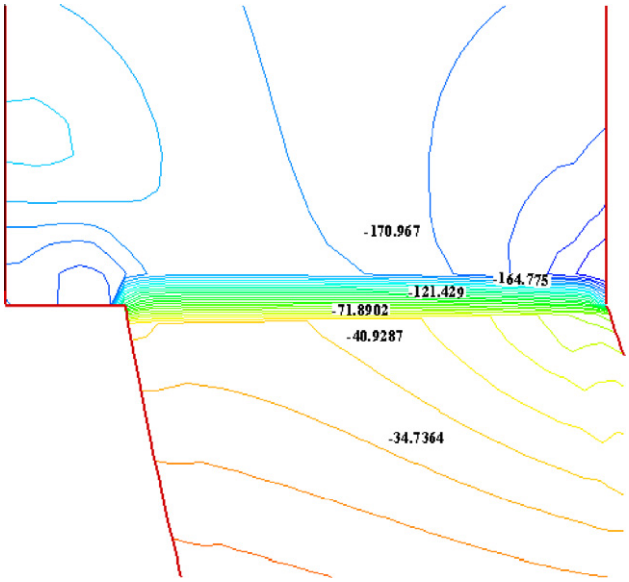


**Fig. 7.** Local relative static pressure distribution near the turbine when the solar radiation and pressure drop across the turbine are 400 W/m$^2$ and 120 Pa, respectively (Pa).

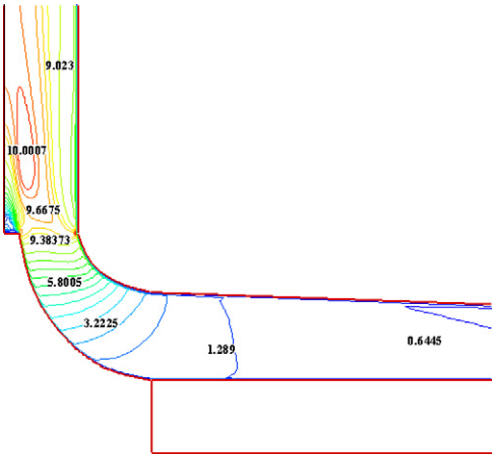


**Fig. 8.** Velocity distribution when the solar radiation and pressure drop across the turbine are 400 W/m$^2$ and 120 Pa, respectively (m/s).

Through comparing the two simulation results corresponding to the turbine pressure drops being 0 Pa and 120 Pa respectively, we found that when the turbine pressure drop increases, the inside–outside pressure difference of the system increases, velocity of the air flow decreases while the temperature of the air flow increases, for which the main reason is that the turbine pressure drop has an inversely effect on the air velocity, thus the heating-up period is prolonged, and the temperature at chimney outlet increases with the pressure drop across the turbine.

Figs. 10 and 11 show the influences of solar radiation and turbine pressure drop on the temperature and velocity at the chimney outlet. As shown in the figures, when the turbine pressure drop increases, the chimney outlet temperature increases while the chimney outlet velocity decreases gradually. This is because the increase of turbine pressure drop causes a block effect to the air flow within the system which makes the air flow rate of the system

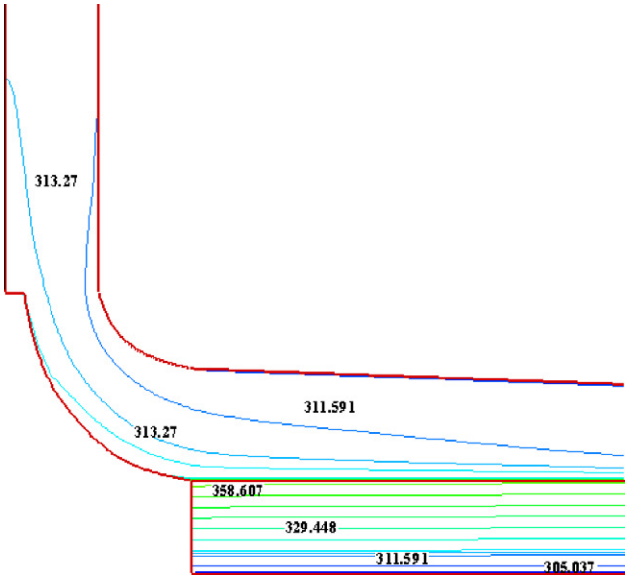


**Fig. 9.** Temperature distribution when the solar radiation and pressure drop across the turbine are 400 W/m$^2$ and 120 Pa, respectively (K).

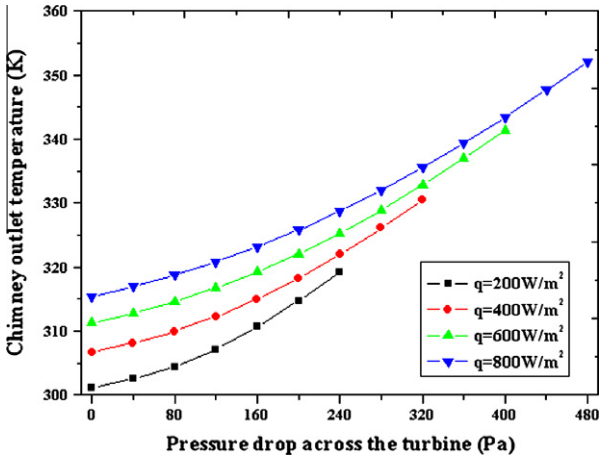


**Fig. 10.** Influences of solar radiation and turbine pressure drop on chimney outlet temperature.

decrease, as a result, the heating-up time of the air inside the collector is prolonged and the chimney outlet temperature increases. Meanwhile, if the turbine pressure drop keeps constant, the air velocity increases notably with the solar radiation, which originates from the relatively high extent to which the fluid is heated during free convection process. Therefore, both the temperature and velocity of the chimney outlet increase.

In general, the air velocities before turbines are often in the scope of 8–9 m/s when wind turbines are on the operation conditions. Based on this scope, it is shown from Fig. 11, corresponding to solar radiation being 200 W/m$^2$, 400 W/m$^2$, 600 W/m$^2$ and 800 W/m$^2$, respectively, that the optimal values of turbine pressure drop are 40 Pa, 120 Pa, 200 Pa and 280 Pa, respectively. As shown in Fig. 10, the variation range for the chimney outlet temperature is 303–333 K under four optimal turbine pressure drops, and the chimney outlet temperature is 320 K when the solar radiation and turbine pressure drop are 600 W/m$^2$ and 200 Pa, respectively.

Fig. 12 indicates the influences of turbine pressure drop and solar radiation on the turbine output power of the SC system, in which the efficiency of turbine is preset as 80%. As shown in the figure, if the turbine pressure drop keeps constant, output power of the system increases with the solar radiation, this is because the increase of solar radiation will result in a notable increase of the system air volume flow rate. However, the influence of turbine pressure drop on the system output power is rather complicated. Under a small turbine pressure drop, the system output power increases with the turbine pressure drop. According to Eq. (14), the main reason for this phenomenon is that the reduction of the air volume flow rate of the system caused by the turbine pressure drop is relatively small, making the product of the air volume flow rate and the pressure drop across the turbine present a rise trend. But when the turbine pressure drop is fairly large, the air volume flow rate decreases more significantly than the extent to which the turbine pressure drop increases, thus resulting in a reduction of the system output power.

Through comparing the simulation results in Fig. 12 and the experimental results of the Spanish SC prototype system Ref. [2], we found that the experimental output power of the Spanish SC prototype system is 35 kW under a solar radiation of about 750 W/m$^2$, while the maximum output power in Fig. 12 is higher than 40 kW under a solar radiation of only 200 W/m$^2$. The main reason for this difference is that the design of the turbine used in Spanish SC prototype system is far from optimization. Form Fig. 12 we can see that the output power of the system by using an optimized turbine will be much higher than that of the Spanish

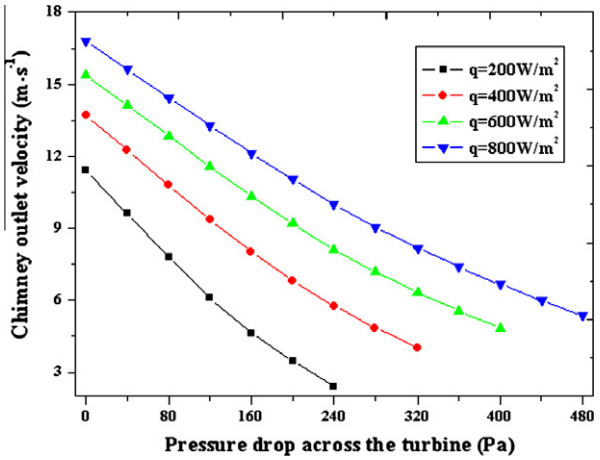


**Fig. 11.** Influences of solar radiation and turbine pressure drop on chimney outlet velocity.

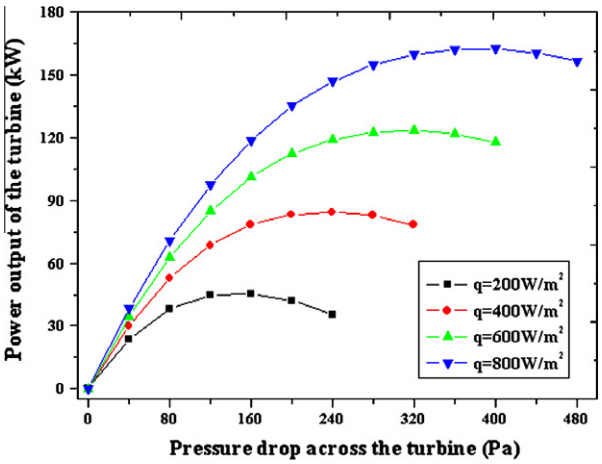


**Fig. 12.** Influences of solar radiation and turbine pressure drop on turbine output power.

SC prototype system when the solar radiation is over 600 W/m$^2$. However, no system output power was reported in Ref. [13] which based its simulation for turbine operation on Beetz theory during the simulation process. On the other hand, as mentioned above, the power efficiency of pressure-based turbine dramatically differs from that of velocity-based free wind field turbine. The simulation results in this work take the turbine as pressure-based, and the turbine efficiency is preset as 80% which is fairly easy to achieve shown in Ref. [10,11], as a result, this brings about relatively a dramatic difference between the theoretical simulation results and the experimental results shown in Ref. [2], which serves as a theoretical law for further optimum design of the turbine coupled with SC system.

Fig. 13 shows the influences of turbine efficiency and turbine pressure drop on the system output power under a solar radiation of 600 W/m$^2$. As shown in this figure, besides the notable influence of turbine pressure drop on the output power of the system, the turbine efficiency also has a notable influence on the output power of the system. With the turbine pressure drop remaining constant, the higher the efficiency of turbine, the larger the output power of the system. Again through comparing the simulation results in this work with the experimental results in Ref. [2], we found that even if the turbine efficiency is only 50%, provided that solar radiation is 600 W/m$^2$ and pressure drop is in a scope of 80–400 Pa, the system output power is always larger than the experimental results shown in Ref. [2]. Therefore, it is concluded that if we increase the turbine efficiency by improve the turbine structure to an optimized design, the system output power will increase remarkably. Besides, Fig. 13 also indicates that the pressure-based turbine of the SC system is able to run in a relatively wide scope of turbine pressure drop with a fairly large system output power.

According to the simulation results as shown in Fig. 12, under a solar radiation of 600 W/m$^2$, the system output power is merely 120 kW even an ideal and optimum designed turbine with a turbine efficiency of 80% is applied. Taking the fact that the component which receives solar radiation within the system is a collector whose radius is 122 m, we can concluded that the total energy conversion efficiency from solar energy to turbine shaft output power is only 0.428%, for which the main reason is possibly excessive energy loss.

When the air flows through the chimney outlet, the total energy loss includes kinetic energy loss, gravitational potential energy and enthalpy, among which the fractional of the kinetic energy and gravitational potential energy are far smaller than the air enthalpy flowing out of the system. These two items of macroscopic energy loss are negligible when calculating energy loss from chimney outlet, thereby the total energy loss from the chimney outlet can be defined as the total enthalpy difference between the chimney outlet and the collector inlet. Fig. 14 shows the influence of turbine pressure drop and solar radiation on energy loss from the chimney outlet. As shown in this figure, energy loss from the chimney outlet is obviously rather large, it is 100–1000 times larger than the output power of the system. It indicates that chimney outlet becomes the most important part of energy loss from the system, when the pressure drop across the turbine is small, the total energy loss from the chimney outlet accounts for 90% of the solar energy received by the system, even when the turbine pressure drop is high, the energy loss from the chimney outlet still accounts for about 75% of total solar energy received by the system, thus resulting in a rather low energy conversion efficiency of the system. Furthermore, we can also see from Fig. 14 that energy loss from the chimney outlet increases significantly with the solar radiation but decreases with the turbine pressure drop which is mainly because the air flow rate decreases dramatically with the turbine pressure drop.

Fig. 15 shows the energy loss from the canopy caused by the turbine pressure drop and the solar radiation. Obviously, energy loss from the canopy increases significantly with pressure drop across the turbine. Under a solar radiation of 200 W/m$^2$ and a pressure drop across the turbine of 200 Pa, the total energy loss from the canopy is nearly 2 MW, namely 50 W/m$^2$ from the system to

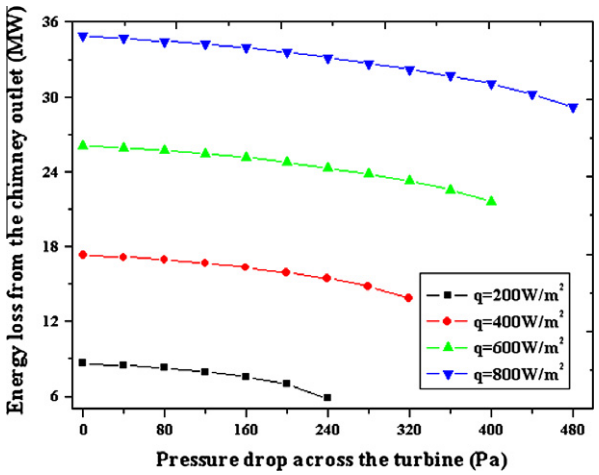


**Fig. 14.** Energy loss from the chimney outlet caused by pressure drop across the turbine.

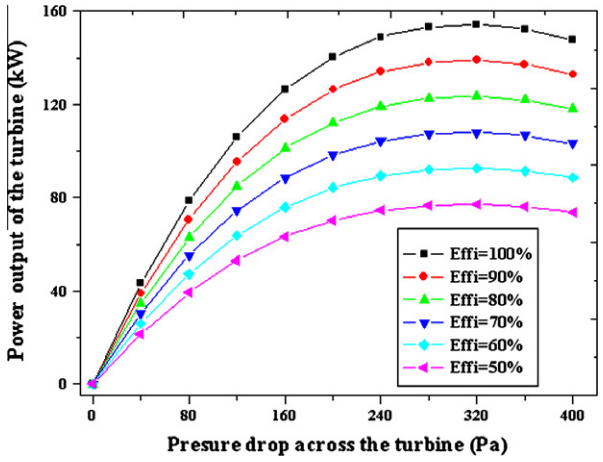


**Fig. 13.** Influences of turbine efficiency and turbine pressure drop on power output of turbine.

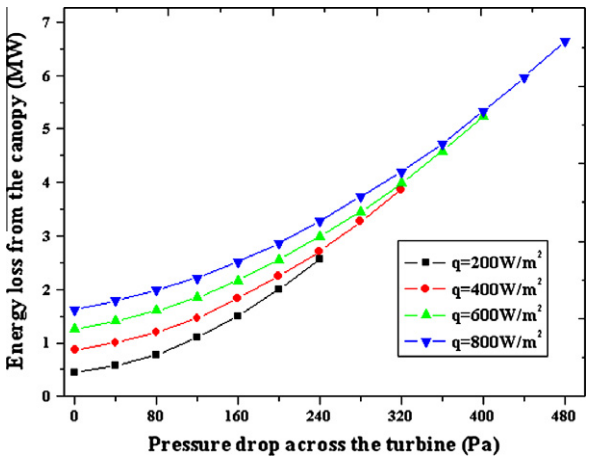


**Fig. 15.** Energy loss from the canopy caused by pressure drop across the turbine.

the environment through the canopy which is nearly 1/4 of the solar radiation intensity; under a solar radiation intensity of 600 W/$m^2$ and a pressure drop across the turbine of 360 Pa, the total energy loss from the canopy is as much as 5 MW, namely 125 W/$m^2$ which is also nearly 1/4 of total solar radiation received. Those mentioned above illustrates that the energy loss from the canopy is also very large, and one way to reduce energy loss from the canopy is to apply a double-layer transparent material, which can effectively reduce energy loss from the canopy.

In addition, numerical simulation results show that the portion of energy loss towards the ground through the energy storage layer is rather small, and is far smaller than the portion of energy loss through the chimney outlet and canopy. When the solar radiation and turbine pressure drop are 600 W/$m^2$ and 360 Pa, respectively, the total energy loss from the bottom of the energy storage layer is only 600 kW. Therefore, the energy loss through the bottom of energy storage layer is negligible when analyzing the total energy loss of SC system.

## 5. Conclusion

Two-dimension steady-state numerical simulations for the solar chimney power plant system, which includes collector, chimney, turbine and energy storage layer, are carried out in this paper. The turbine is regarded as a pressure-based one which is different from that in Ref. [13] and the energy storage layer is treated as porous media as mentioned in Ref. [14], aiming at analyzing the pressure, velocity and temperature distributions of the system. Meanwhile, the influence of the turbine pressure drop on the flow and heat transfer characteristics and the output power of the SC system are considered. Besides, the influences of solar radiation and turbine efficiency on the output power and energy loss of the system are also analyzed. Through analysis, it is found that the influences of solar radiation and pressure drop across the turbine are rather considerable; large outflow of heated fluid from the chimney outlet becomes the main cause for the energy loss of the system, and canopy also causes considerable energy loss.

## References

[1] Haaf W, Friedrich K, Mayer G, Schlaich J. Solar chimneys. Int J Solar Energy 1983;2:3–20.
[2] Haaf W, Friedrich K, Mayer G, Schlaich J. Solar chimneys. Int J Solar Energy 1984;2:141–61.
[3] Kulunk H. In: Veiroglu TN, editor. A prototype solar convection chimney operated under Izmit conditions. Prod. 7th MICAS 162; 1985.
[4] Pasumarthi N, Sherif SA. Experimental and theoretical performance of a demonstration solar chimney model – Part I: experimental and theoretical results and economic analysis. Int J Energy Res 1998;22:443–61.
[5] Pasumarthi N, Sherif SA. Experimental and theoretical performance of a demonstration solar chimney model – part II: mathematical model development. Int J Energy Res 1998;22:277–88.
[6] Bernardes MA, Vob A, Weinrebe G. Thermal and technical analyzes of solar chimneys. Solar Energy 2003;75(3):511–24.
[7] Bilgen E, Rheault J. Solar chimney power plants for high latitudes. Solar Energy 2006;79:449–58.
[8] Pretorius JP, Kröger DG. Critical evaluation of solar chimney power plant performance. Solar Energy 2006;80:535–44.
[9] Gannon AJ, Von Backström TW. Solar chimney cycle analysis with system loss and solar collector performance. J Solar Energy Eng 2000;122:133–7.
[10] Gannon AJ, Von Backström TW. Solar chimney turbine performance. ASME J Solar Energy Eng 2003;125:101–6.
[11] Von Backström TW, Gannon AJ. Solar chimney turbine characteristics. Solar Energy 2004;76:235–41.
[12] Pastohr H, Kornadt O, Gurlebeck K. Numerical and analytical calculations of the temperature and flow field in the upwind power plant. Int J Energy Res 2004;28(3):495–510.
[13] Ming TZ, Liu W, Xu GL. Analytical and numerical simulation of the solar chimney power plant systems. Int J Energy Res 2006;30(11):861–73.
[14] Ming TZ, Liu W, Pan Y, et al. Numerical analysis of flow and heat transfer characteristics in solar chimney power plants with energy storage layer. Energy Convers Manage 2008;49:2872–9.
[15] Ming TZ, Liu W, Xu GL, et al. Numerical simulation of the solar chimney power plant systems coupled with turbine. Renew Energy 2008;33(5):897–905.
[16] Sung JK, Christopher YC. Convective heat transfer in porous and overlying fluid layers heated from below. Int J Heat Mass Transfer 1996;39(2):319–29.
[17] Fluent Inc. Fluent user's guide; 2006.